Eclipse Timings of the Low Mass X-ray Binary EXO 0748–676 III. An Apparent Orbital Period Glitch Observed with USA and RXTE

Michael T. Wolff[1], Paul Hertz[2], Kent S. Wood, Paul S. Ray

and

Reba M. Bandyopadhyay[3,4]

E. O. Hulburt Center for Space Research, Naval Research Laboratory, Washington, DC 20375

ABSTRACT

We present 7 eclipse timings of the low mass X-ray binary EXO 0748−676 obtained with the USA experiment during 1999−2000 as well as 122 eclipse timings obtained with RXTE during 1996−2000. According to our analysis, the mean orbital period has *increased* by ∼ 8 ms between the pre-RXTE era (1985−1990) and the RXTE/USA era (1996−2000). This corresponds to an orbital period derivative of $P_{\rm orb}/\dot{P}_{\rm orb} \sim 2 \times 10^7$ years. However, neither a constant orbital period derivative nor any other simple ephemeris provides an acceptable fit to the data: individual timings of eclipse centers have residuals of up to 15 or more seconds away from our derived smooth ephemerides. When we consider all published eclipse timing data including those presented here, a model that includes observational measurement error, cumulative period jitter, and underlying period evolution is found to be consistent with the timing data. We discuss several physical mechanisms for LMXB orbital evolution in an effort to account for the change in orbital period and the observed intrinsic jitter in the mid-eclipse times.

Subject headings: binaries: eclipsing, stars: individual: EXO 0748−676, binaries: X-ray

---

[1]E-mail Address: Michael.Wolff@nrl.navy.mil

[2]Now at the Office of Space Science, NASA Headquarters

[3]NRC/NRL Cooperative Research Associate

[4]Now at the Department of Astrophysics, Oxford University

1.   Introduction

The physical process that drives the accretion in low mass X-ray binary (LMXB) systems is not known with any certainty. The accretion may be driven by the loss of orbital angular momentum through gravitational radiation, by the loss of orbital angular momentum through magnetic braking, or by the nuclear evolution of the secondary causing it to overflow its Roche lobe. The mass transfer from the donor star to the compact object can be either conservative or non-conservative. Models incorporating these physical processes make specific predictions for the rate at which the system orbital period (P_{orb}) changes. For instance, P_{orb} of an LMXB undergoing conservative mass transfer at typically observed accretion rates (10^{-10} to 10^{-8} $M_\odot$ yr^{-1}) from a Roche-lobe-filling, 1 $M_\odot$ main sequence secondary is expected to decrease with a time scale of 10^8 to 10^{10} years (Rappaport et al. 1982). Thus, measuring the orbital period derivative ($\dot{P}_{orb}$) should provide a fundamental diagnostic of the evolution of LMXB systems. Unfortunately, none of the reported orbital period derivatives in LMXBs are in agreement with theoretical expectations (Tavani 1991; White et al. 1995).

Six LMXB systems are currently reported to have observed orbital period derivatives. Three of these systems (X1820−303, X1658−298, and Her X-1) have apparently negative period derivatives implying that the orbital separation is shrinking (van der Klis et al. 1993; Wachter et al. 2000; Deeter et al. 1991). In each of these systems the orbit period measurements imply orbital evolution that is proceeding considerably faster (by 1–2 orders of magnitude) than theoretical predictions for systems undergoing conservative mass transfer (e.g. see the discussion in White et al. 1995). However, for two of these systems (X1820−303 and Her X-1) it is doubtful that the "standard picture" of LMXB evolution is applicable. X1820−303 has the shortest orbital period of any LMXB currently known (11 minutes), the mass donating secondary is believed to be a white dwarf, and it resides in the globular cluster NGC 6624, making its orbital dynamics particularly difficult to understand (van der Klis et al. 1993). Her X-1 has a 2.2 $M_\odot$ companion and is an X-ray pulsar so it is not generally representative of LMXBs (Deeter et al. 1991). On the other hand, the transient low mass X-ray binary X1658−298, which resumed its persistent X-ray emission in 1999 April 2 after a 21-year quiescence, does appear to have a low-mass donor star, is a prodigious burster, shows kHz quasiperiodic X-ray oscillations, and shows regular total eclipses in its X-ray light curve (Cominsky & Wood 1984, 1989; Wachter & Smale 1998; Wijnands et al. 2001; Wachter et al. 2000). Thus it appears to be a "normal" LMXB. When the extensive Rossi X-Ray Timing Explorer (RXTE) observations of X1658−298 eclipses are combined with eclipse observations from its previous outburst epoch (Cominsky & Wood 1989) the results show that the 7.1-hr orbital period of the system has *apparently* decreased by $\sim$ 11 milliseconds (Wachter et al. 2000). This implies an orbital evolutionary time scale of $\tau_{orb} \sim |P_{orb}/\dot{P}_{orb}| \sim 10^7$ years, and is of a magnitude similar to other cases of LMXB orbital period evolution despite the fact

that little or no mass transfer is thought to have occurred during the interval $1978-1999$. On the other hand, Oosterbroek et al. (2001) added two mid-eclipse timings based on BeppoSAX observations to the record for X1658$-$298 and concluded that the large $\dot{P}_{\rm orb}$ reported by (Wachter et al. 2000) may be an artifact of the non-uniform sampling of the timing data for this source. Thus, whether or not the orbit in X1658$-$298 is evolving at an observable rate is still an open question.

In three other LMXB systems (X1822$-$371, X2127+119, and EXO 0748$-$676) the orbital period derivative is apparently positive, implying that the binary orbital separation is increasing. The system X2127+119 in the globular cluster M15 has an observed $\tau_{\rm orb} \sim 10^6$ years, leading Homer & Charles (1998) to conclude that it was in the midst of a transient super-Eddington accretion episode. Heinz & Nowak (2001) studied X1822-371 and derived an orbital evolution time scale of $\tau_{\rm orb} \sim 3.6 \times 10^6$ years, forcing them to conclude as well that it was in the midst of a short-lived mass exchange episode. These two systems, however, only show partial eclipses that must be fitted with Gaussian profiles in the light curve variations in order to determine the times of phase 0 for each orbit cycle (Homer & Charles 1998; Heinz & Nowak 2001). Such a procedure has very large error estimates and this makes the observational determination of their orbit period evolution more uncertain than the case of either X1658$-$298 or EXO 0748$-$676.

The LMXB EXO 0748$-$676 is a 3.82 hr eclipsing binary system with a neutron star primary accreting matter from the Roche lobe-filling, low-mass main-sequence secondary star UY Vol. This source exhibits Type 1 X-ray bursts (Gottwald et al. 1986; Gottwald et al. 1987), quasi-regular X-ray dips (Smale et al. 1992; Church et al. 1998), 1 Hz quasiperiodic oscillations (Homan & van der Klis 2000) and kHz quasiperiodic oscillations (Homan et al. 1999), interesting spectral variability (Thomas et al. 1997), and complete periodic X-ray eclipses (Parmar et al. 1986). It is this last property which makes EXO 0748$-$676 important as there are only three known LMXBs [EXO 0748$-$676, X1658$-$298, and the recently discovered XTE J1710$-$281 (Markwardt et al. 2002)] showing full eclipses of the compact object X-ray source. Eclipsing systems allow the best chance of detecting the expected orbital period evolution in LMXB systems because the eclipse transitions should provide accurate fiducial timing marks. However, each time new eclipse timings of EXO 0748$-$676 have been made, new conclusions have been drawn about its orbital period. These include a constant $P_{\rm orb}$ (Parmar et al. 1986), decreasing $P_{\rm orb}$ (Parmar et al. 1991), increasing $P_{\rm orb}$ (Asai et al. 1992), sinusoidal $P_{\rm orb}$ (Corbet et al. 1994), constant $P_{\rm orb}$ with intrinsic variability (Hertz et al. 1995, hereafter Paper I), and increasing $P_{\rm orb}$ with intrinsic variability (Hertz et al. 1997, hereafter Paper II).

The usual manner in which orbital period evolution in eclipsing binaries has been tracked

is to observe a small number of eclipses spaced closely as a group but widely separated in time from previous measurements (typically by many months or even years). This is done so that a long time baseline can be established on which to track any observed changes with a reasonable allocation of observing time. The measured eclipse times are often fit to a model using a standard $O - C$ (observed $-$ calculated) analysis which is basically a least-squares fit to a parameterized timing model. However, Lombard & Koen (1993) have argued that this process can be misleading. If there is some intrinsic process that subjects P_{orb} to small random fluctuations around a mean P_{orb} (which we will refer to as "intrinsic period jitter"), this can be misinterpreted as a non-zero $\dot{P}_{orb}$, even if the underlying P_{orb} is constant. Sparse sampling exacerbates this problem since it can mask the resulting random walk character of the $O - C$ residuals. More sophisticated analysis methods (e.g., Koen 1996) than the standard $O - C$ method are required to place confidence limits on the underlying orbital period derivative in the presence of such intrinsic period jitter.

What is clear is that more than 20 years of monitoring of LMXB orbital evolution has failed to show any LMXB displaying orbital evolution that is either consistent with theoretical predictions or that can be characterized by simple mathematical descriptions. Beginning with the launch of RXTE in 1996 we began a program of monitoring EXO 0748−676 in an effort to closely scrutinize its orbital period evolution. This program consists of closely grouped observations of up to 6 eclipses with each group spaced at 2 to 3 month intervals throughout the year. The launch of the *Advanced Research and Global Observation Satellite* (ARGOS) carrying the Unconventional Stellar Aspect (USA) experiment further increased the possibilities for eclipse observations. We discuss the relevant technical aspects of our observations in §2.

We report here on 7 new eclipse timings determined with USA and 122 new eclipse timings for EXO 0748−676 obtained during 1996−2000 with RXTE. Combined with the data reported in Paper II, we now have 4 years of frequent, accurate (eclipse center timing uncertainty < 1 s) eclipse timings. We show in §3 that the accurately determined orbital period during the time interval 1996−2000 appears significantly different than the orbital period observed during the interval 1985−1990. Cycle count has been maintained over the entire 15 years and we continue to observe significant residuals in eclipse timings when mid-eclipse times are compared with simple orbital ephemerides similar to those reported in Paper I. We significantly update the maximum likelihood method (MLM) determination of the period evolution over that of Paper II in §4. MLM solutions for the orbit dynamics require both orbital period evolution and intrinsic period jitter in addition to uncorrelated random measurement errors. In §5 we discuss the observed period evolution and possible physical mechanisms that may help account for the difference between our results and the current state of the theoretical models.

2. Observations

All of the new observations we present here were made either with the Proportional Counter Array (PCA) on RXTE or the USA detector on ARGOS.

2.1. RXTE Observations

The PCA is an array of five large-area X-ray proportional counters (Proportional Counter Units or PCUs) with microsecond time resolution (Jahoda et al. 1996). We have conducted a continuing program with the PCA to observe and time EXO 0748−676 eclipses with sub-second timing resolution. The resolution we obtain is limited primarily by counting statistics in the X-ray flux and any intrinsic variability in the X-ray emission from the neutron star. In the 2-8 keV band the un-eclipsed source flux is typically $\sim 15 - 25$ counts s^{-1} PCU^{-1}, which is larger than the PCA background in that band ($\sim 3 - 5$ counts s^{-1} PCU^{-1}). We restrict our analysis to this energy range because it provides the best signal–to–noise for our analysis. We have conducted 4 to 6 observing campaigns per year since 1996 with the PCA. During each campaign we observe up to 6 complete eclipses (starting before ingress and observing until after egress) of EXO 0748−676 over roughly a one day period. If RXTE scheduling considerations allow it, that interval can include a number of consecutive eclipses.

A log of our observing campaigns with RXTE is given in Table 1. For each eclipse we determine the cycle number (N) according to the cycle numbering system initiated by Parmar et al. (1991) but with an updated solution for the mid-eclipse time for cycle 0: $T_0(\mathrm{TDB;MJD}) = 46111.07418607$ and $P_{\mathrm{orb}} = 0.159337819$ days. The results from the first two campaigns (N $= 25702 - 26358$) were reported in Paper II. For the first three campaigns (N $= 25702 - 26660$) we obtained 32 ms resolution binned data with no detector layer identification (the *E_8US_32B_0_1S* mode of the PCA EDS data system). For the remaining campaigns we recorded individual photon event data (the *GoodXenon* EDS mode).

Each RXTE observation is processed in a standard manner using scripts which call modules of the FTOOLS data analysis package. Our analysis technique allows each eclipse to be independently processed in exactly the same manner. The script performs the following analysis functions: (i) The data are filtered for quality and we eliminate observations where the data are incomplete, where bursts occur at any time near enough to the eclipse to affect its observed profile, and where the background contamination is large. (ii) Where possible (i.e., after the first three campaigns), we extract only layer 1 data in channels 7–21 which corresponds to an energy range of 2–8 keV. Because we are interested in timing of eclipses, our results should be independent of energy-channel boundary considerations. Thus, we

make no adjustment in our analysis technique across gain-epoch boundaries. If some of the PCUs were turned on and/or off during an observation but far from the eclipse, we extract data only from PCUs that were on during the entire observation. (iii) We bin the data in 0.5 s bins (unless otherwise noted below) and correct the timing markers to the solar system barycenter. We use the FTOOL "faxbary" which gives us increased timing resolution over that provided by the barycentering tool "fxbary." Thus, our data achieve an absolute timing accuracy of better than 100 μs (see Rots et al. 1998) which is entirely adequate for our purposes. (iv) We calculate and subtract the faint source PCA background model for the epoch of that particular observation from the binned light curves. (v) We fit a model eclipse light curve to each background subtracted, barycenter corrected, binned light curve.

The model light curve is the standard piecewise linear ramp-and-step model similar to that used by all investigations which timed EXO 0748−676 eclipses (e.g. Parmar et al. 1991). The model has seven free parameters: flux before ingress, duration of ingress, flux during eclipse, duration of eclipse, time of mid-eclipse, flux after egress, and duration of egress. The eclipse fitting routines calculate the best model parameters using Marquardt's method (Press et al. 1992). Our procedure is to first do a complete fit to all seven parameters in our model and then with careful refined searching, locate the χ^2 minimum as a function of mid-eclipse time. The errors in our mid-eclipse times are estimated by stepping away from the χ^2 minimum in the mid-eclipse time until we reach the change in this time that corresponds to an increase in the χ^2 statistic by 1.0 over its minimum value, refitting only the other six model parameters at each step. This procedure yields the experimental 68% confidence interval for the single fitted parameter that we are interested in here: the time of mid-eclipse.

2.2. USA Observations

The USA X-ray timing experiment is a two X-ray proportional counter instrument on the Air Force's ARGOS satellite. ARGOS was launched on February 23, 1999, into a sun-synchronous polar orbit from Vandenberg Air Force Base. Each USA detector is a thin window proportional counter with sensitivity between 0.5 and 25 keV and a peak effective area of 1100 cm^2 (Wood et al. 1999; Ray et al. 2001). On June 8, 1999, detector 2 of USA failed due to a gas leak. All of the data reported here was taken with a single proportional counter. On November 17, 2000, the gas system in detector 1 failed as well, effectively ending the X-ray observational part of the USA mission.

An ongoing USA campaign to observe several EXO 0748−676 eclipses a week was begun on January 9, 2000. The USA observations of EXO 0748−676 provide photon event data with

32 μs resolution (USA Science Mode 1). The ARGOS polar orbit limits USA observations to exposures which are shorter than ~ 1100 seconds, so observing complete eclipses is difficult but not impossible. Generally the phase of the ARGOS/USA orbit allows the observation of either an eclipse ingress or egress, and if the orbit happens to be very well-phased to the orbit of the EXO 0748−676 system, a complete eclipse. Thus, the USA observation database has numerous short observations that include either an ingress or an egress. The observations we present here are 7 observations which included full eclipses. In Table 2 we give a list of USA observations of full eclipses included in our analysis. The USA orbital constraints also make it impossible to observe consecutive (ΔN = 1) EXO 0748−676 eclipses.

For each observation, we have binned the data into 1.0 s bins (unless otherwise noted below) and corrected the timing markers to the solar system barycenter including all relevant solar system corrections from the DE200 ephemeris. The ARGOS satellite positional accuracy is sufficient to provide us with absolute timing accuracy to better than 300 μs, which is again good enough for our purposes (Ray et al. 2000). Once the usable sections of data are identified we can proceed for the USA observations in the same manner as for the RXTE observations. We fit the same type of seven-parameter linear ramp-and-step model as in the RXTE case to the full eclipses observed by USA.

2.3. Other Published Data

Numerous other investigations have been made of the orbital ephemeris of EXO 0748−676 and we have incorporated those data in several places in our analysis. We have taken 30 EXOSAT mid-eclipse times and one GINGA mid-eclipse time from Parmar et al. (1991), eight GINGA mid-eclipse times from Asai et al. (1992), four ASCA mid-eclipse times from Corbet et al. (1994), and one ROSAT timing from Hertz et al. (1994). This yields an additional 44 mid-eclipse timings dating back to February 1985. These data are listed in Table 3 for completeness. Where appropriate, we have adjusted the given UTC-based barycenter corrected times to the TT time system by adding the correct number of leap seconds and adding the 32.184 second difference between the TAI and TT time systems. In most cases we have adopted the errors stated in those papers except that we assign a uniform error of 1.5 seconds to the Corbet et al. 1994 points. Thus, when we refer to "All Data" all the times incorporated in our analysis are on the same time system and thus directly comparable.

3.   Orbital Ephemerides

In Figure 1 we show a traditional $O - C$ diagram (observed minus calculated mid-eclipse time) for the USA and RXTE EXO 0748−676 eclipse timings from Tables 1 and 2 where the calculated times are the best-fit constant period ephemeris (given in Table 4). The error bars in the figure represent the *measurement errors* for each observation as determined in §2.1. The fit is formally very poor, with a reduced χ^2 statistic of 84.8 per degree of freedom (dof) for 127 dof. The rms scatter in the residuals is 2.94 seconds which is much larger than the rms standard measurement uncertainty of 0.47 seconds. There is clearly significant variability in the measured mid-eclipse times about the ephemeris. The variation in the $O - C$ values can not be explained by simple measurement error. When the USA and RXTE data (1996−2000) are fitted with a non-zero $\dot{P}_{\mathrm{orb}}$ model the best fit shows a *negative* (P_{orb} decreasing) period derivative. This fit is also very poor (see the solid curve in Figure 1) with $\chi^2/\mathrm{dof} = 68.0$, almost as large as the constant P_{orb} case. The rms scatter of the residuals is now 2.78 s.

In Figure 2 we show the $O - C$ residuals to a same constant period model for *all* published mid-eclipse timings of EXO 0748−676. Obviously, a constant period model is unacceptable. The EXOSAT points have $O - C$ residuals of 75–90 seconds relative to the constant period ephemeris. A constant $\dot{P}_{\mathrm{orb}}$ model (whose parameters are in Table 4) is also a poor fit to the data with a reduced χ^2 of 121.1 with 170 dof. The residuals in Figure 2 also might be interpreted as evidence for a sudden period change around 1990. Thus, we have also fitted a two–period model to the data in which we constrain the phase to be constant across the instantaneous period change but let the cycle of the period change be a free parameter. The best fit two–period model is given as the last model in Table 4. In that model, $P_{\mathrm{orb},1}$ is tightly constrained by the large number and high precision of the RXTE observations. The change in period is $P_{\mathrm{orb},1} - P_{\mathrm{orb},0} = 7.87 \pm 0.06$ ms. However, even this model is a statistically poor fit to the timing residuals with a reduced $\chi^2/\mathrm{dof} = 67.3$ for 169 dof. Furthermore, as we show below, it is likely that the "sudden" period change is simply an artifact of the much sparser sampling in the older data.

4.   Observed Intrinsic Period Jitter and Eclipse Profile Changes

4.1.   Maximum Likelihood Analysis

During the epoch covered by the RXTE and USA observations, 1996–2000, there are significant residuals in the mid-eclipse timings about a constant period. These residuals can appear on time scales as short as a single orbital cycle: the observed change in orbit period as determined across consecutive mid-eclipse timing fits differs by over 11 seconds,

ranging from 0.02 ± 0.29 for cycles 25704–25706 to 11.38 ± 0.53 s for cycles 34938–34940. Furthermore, just as was found in Paper II, the $O - C$ residuals in Figure 1 and Figure 2 are strongly correlated. In Paper II we pointed out that apparent changes in orbital period can be caused by cumulative intrinsic jitter in a system with constant mean orbital period. We make a distinction here between "measurement error" and "intrinsic period jitter" in the mid-eclipse timings. Measurement error is the random, uncorrelated error associated with our measurement of the individual mid-eclipse times and is dominated by counting statistics and short time-scale ($\sim$seconds) fluctuations of the source flux that degrade the accuracy of our measured eclipse profiles. On the other hand, by intrinsic jitter we mean a cumulative process where the orbital period for any particular cycle suffers small random (zero mean) fluctuations around the true underlying orbital period. If the underlying model used to compute the predicted eclipse times is correct, then the $O - C$ residuals can be represented as

$$(O - C)_j = \sum_{i=1}^{N_j} \epsilon_i + e_j, \tag{1}$$

where ϵ_i is a random, zero-mean, fluctuation in the length of orbit period i and e_j is the measurement error in the jth mid-eclipse time (Koen 1996). The cumulative nature of the ϵ_i causes the systematic wandering of the mid-eclipse residuals apparent in Figure 1. In other words, the mid-eclipse times are doing a random walk about the times that would be predicted from the "true" orbital period.

We have used Koen's (1996) maximum likelihood method (MLM) to estimate the parameters of a model for the orbital evolution that simultaneously includes an orbital period, an orbital period derivative, intrinsic period jitter, and random measurement error. In Paper II we applied a similar method to a small subset of these data. In the present analysis we include all eclipse timings given in Tables 1 and 2 as well as all previously published eclipse timings given in Table 3 for a total of 173 mid-eclipse times. In the MLM method a likelihood ratio statistic is used to determine how important a certain parameter is in fitting these data. The observed mid-eclipse timings are represented by $T_0, T_1, T_2, ..., T_J$, corresponding to cycle numbers $N_0, N_1, N_2, ..., N_J$, where J is the number of observed eclipse centers. The time intervals between successive eclipse centers are given by $y_j = T_j - T_{j-1}$, with each interval accounting for $n_j = N_j - N_{j-1}$ cycles. If a linear form is assumed for the period evolution then it is easy to show that the y_j can be written as

$$y_j = n_j P_{orb} + m_j \Delta + \sum_{i=N_{j-1}+1}^{N_j} \epsilon_i + e_j - e_{j-1}, \tag{2}$$

where $m_j = n_j(2N_j - n_j + 1)/2$, $\Delta = P_{\rm orb}\dot{P}_{\rm orb}$, e_j is the observational measurement error for cycle j, and ϵ_j is the intrinsic jitter in the mid-eclipse timing for cycle j. The MLM method

consists of solving a linear system of J equations for the maximum likelihood estimates for the orbit period P_{orb}, the orbit period derivative Δ, the measurement error variance σ_e^2, and $q \equiv \sigma_\epsilon^2/\sigma_e^2$, where σ_ϵ^2 is the variance of the intrinsic jitter. For a particular value of q one can define the logarithm of the likelihood function by

$$\ln L(H_i) = -\frac{1}{2}[J\ln(2\pi) + J\ln(\sigma_e^2) + \ln|\Sigma_*| + J],\tag{3}$$

where the $L(H_i)$ represents the likelihood of the particular hypothesis (i) one is testing, and Σ_* is the covariance matrix for the y-values divided by the measurement error variance (see Koen 1996 for details). The "full" model consists of a representation of the data in which each of the four parameters, σ_e^2, σ_ϵ^2, P_{orb}, and Δ, take on non-zero values and is labeled hypothesis H_0. This model is determined by iterating on the value of q until $\ln L(H_0)$ attains its maximum value. Once the full model is found it can be compared with model solutions for which either the orbital period derivative is zero ($\Delta = 0$; hypothesis H_1), or the intrinsic jitter (σ_ϵ^2) is zero ($q = 0$; hypothesis H_2). The likelihood ratio statistic

$$\lambda_k \equiv 2[\ln L(H_0) - \ln L(H_k)] \ \text{ for } k = 1, 2,\tag{4}$$

then gives a measure of the likelihood of the full model relative to one of the null hypotheses.

In Table 5 we give results for two cases: (1) all data including the USA and RXTE timings, and, (2) the USA and RXTE data only. For case (1) the preferred model is a model that includes both non-zero intrinsic period jitter ($\sigma_\epsilon > 0$) and period evolution ($\dot{P}_{\text{orb}} \neq 0$). A model for the full data set that has no period evolution is rejected relative to the full model at the 99.86% ($e^{-7.16}$) confidence level ($\lambda_1 = 10.16$) and a model with no intrinsic jitter is rejected when compared to the full model at the $\gg$ 99.999% ($e^{-207.8}$) confidence level ($\lambda_2 = 407.7$). For case (2), where only the 1996$-$2000 USA and RXTE data are considered, the results are not so clear. A model with no period evolution ($\Delta = 0$) but non-zero intrinsic jitter is only rejected at the relatively weak 90.3% ($e^{-2.80}$) confidence level compared to the full model ($\lambda_1 = 2.76$). Again, however, a model with no intrinsic jitter is strongly rejected at the $\gg$ 99.999% ($e^{-41.6}$) confidence level ($\lambda_2 = 76.9$). Furthermore, the derived $\dot{P}_{\text{orb}}$ from the full model for the RXTE and USA case is negative just as it was for the simple χ^2 fitting in the previous section and this is contrary to the results for $\dot{P}_{\text{orb}}$ when all eclipse data are included. These results indicate that during the RXTE and USA era, because of the apparent intrinsic period jitter, the mid-eclipse timing data are insufficient to clearly determine the true long-term behavior of the orbit period in EXO 0748$-$676. The intrinsic jitter in the eclipse timings contributes significantly to the apparent variation in the orbit period over the past 4 years. For this system at least, the intrinsic jitter appears to mask the underlying orbit period behavior over multi-year time scales.

There is one important caveat that must be mentioned in evaluating the MLM analysis above, however. In deriving Equation (4) the assumption is made that both the measurement error and the intrinsic jitter are independent and normally distributed random variables. For the measurement error this is a reasonable assumption but for the intrinsic jitter the situation is less clear. In Figure 3 we see that the $O - C$ residuals for 73 pairs of observed consecutive eclipses during the RXTE and USA era are scattered around a mean difference of 0.061 seconds with a standard deviation is 2.21 seconds. The amplitude of the point-to-point variations in this figure is determined by the sum of the measurement error and the intrinsic jitter. This level of variation is close to the sum of the measurement error and intrinsic jitter from either the MLM full model or the no period evolution model in the case of the RXTE and USA data only (see Table 5). Thus, based on these data, we can not determine if the intrinsic jitter is truly random and independent because any variations would be swamped by the measurement error in this figure unless they were very large. But we can observe that if the period varied in some systematic way during the RXTE/USA era due to large variations in the intrinsic jitter then a shift away from a mean of zero with time would be apparent in the figure but no shift is observed. Furthermore, if the magnitude in the intrinsic jitter changed dramatically during the RXTE/USA era then the amplitude of the variations in the figure would reflect this but again no such effect is observed. An independent check on the properties of the intrinsic jitter must await the observation of substantially more eclipses than we present here.

Finally, we note that the eclipse profiles can be quite variable. We define the ingress and egress durations as the time it takes for the observed count rate to go from the pre-transition count rate to the post-transition rate, and the eclipse duration as the time from the end of ingress to the beginning of egress. With these definitions we find that the RXTE and USA observed eclipse durations vary between 482 s and 511 s during $1996-2000$ (Figure 4) with mean 497.5 ± 6.0 s, while the average duration of the EXOSAT-observed eclipses in $1985-1986$ was 492.5 ± 5.0 s (Parmar et al. 1991; Figure 5). The duration of ingress and egress varies as well with observed ranges between 1.5 s and 40 s for EXOSAT and RXTE observed eclipses (Figure 6). The EXOSAT observed eclipse transitions averaged about 11.7 s, and the RXTE observed eclipse transitions averaged about 7.5 s in duration. There appears to be a slow downward trend in the eclipse duration during the RXTE/USA era apparent in Figure 4. We note, however, that the eclipse durations appear to be uncorrelated with other system eclipse parameters (e.g., the durations of either ingress or egress transitions) during this era. This variability and the intrinsic variability of the X-ray source being eclipsed contribute to the uncorrelated random error and explain why the measured σ_e is larger than the measurement errors derived from the eclipse fits.

4.2. Monte Carlo Illustration

To illustrate how the a random walk and sparse sampling can interact to exhibit the behavior we have seen in the EXO 0748−676 residuals, we have made a simple Monte Carlo simulation which implements Equation 1 for a simulated eclipsing system. We assume that the system has no underlying orbital period derivative and that observed mid-eclipse times are subject to both measurement error and intrinsic period jitter. In Figure 7 we show both the full simulated dataset and one that has been subjected to the same sampling function as the actual EXO 0748−676 measurements. Comparing this to Figure 2 demonstrates how such a simple model can replicate the behavior we observe in a real system. Looking at the sparsely sampled data one could easily see, or fit, spurious period derivatives, sudden period changes, or other phenomena that are caused by the random walk and are not present in the underlying period evolution (to which the random walk will always return over long time scales). Furthermore, when we take the results for the eclipse timings from our Monte Carlo simulations, with a sampling function that represents the real sampling of the EXO 0748−676 eclipses, and apply the MLM analysis technique to these data we recover the approximate intrinsic jitter magnitude and the estimated measurement error magnitude we used as inputs to the Monte Carlo model. This demonstrates that the MLM results are a valid representation of the timing data. Since there was no $\dot{P}_{\mathrm{orb}}$ in the Monte Carlo simulations, the MLM technique should not indicate a preference for a non-zero $\dot{P}_{\mathrm{orb}}$ and this is indeed the case. In the case of the real EXO 0748−676 data the MLM model indicates that the random walk is unlikely to be able to fully account for the ~ 90 second residuals observed in the EXOSAT era, and thus a model with some period evolution plus the intrinsic jitter is preferred.

5. Discussion

Based on our analysis above we conclude that the EXO 0748−676 orbital period has increased by ~ 8 ms over the past 16 years. This measured $\dot{P}_{\mathrm{orb}}$ implies that the two stellar components of EXO 0748−676 are moving away from each other instead of toward each other as our current theoretical understanding of LMXB orbit evolution indicates they should (Rappaport et al. 1982; Tavani 1991; Verbunt & van den Heuvel 1995). Furthermore, the intrinsic period jitter that we conclude causes the measured mid-eclipse times to do a random walk in the $O - C$ diagram is certainly not expected from previous theoretical work, but we are forced, by the data, to conclude that it is present at the level of ~ 0.1 s per cycle. We now turn to some possible explanations for the behavior we observe in EXO 0748−676.

5.1. A Positive Orbital Period Derivative?

Mass capture by the compact object in EXO 0748−676 can lead to a positive $\dot{P}_{\rm orb}$ as we show with a simple model. If the stellar component spin angular momentum is negligible and the orbital eccentricity is zero, the total system angular momentum consists of only orbital angular momentum which we can write as

$$J_{\rm orb} = \sqrt{\frac{GaM_1^2 M_2^2}{M_1 + M_2}} \; , \tag{5}$$

where M_1 is the mass of the primary star (the compact object) that accretes and M_2 is the mass of the secondary mass-losing star, a is the orbital separation and G is the gravitational constant. Differentiating equation (5), using Kepler's Law, and assuming conservative mass transfer gives

$$\frac{\dot{P}_{\rm orb}}{P_{\rm orb}} = \frac{3}{J_{\rm orb}} \left(\frac{\partial J_{\rm orb}}{\partial t} \right)_{GR} - \frac{3\dot{M}_2}{M_2} \left[1 - \frac{M_2}{M_1} \right], \tag{6}$$

where the first term represents the loss of system angular momentum to gravitational radiation and $\dot{M}_2$ is the mass loss rate from the secondary star. We ignore magnetic braking here since the interior of the low mass secondary is likely to be completely convective and magnetic braking under such circumstances is believed to be suppressed (Verbunt & van den Heuvel 1995). In Figure 8 we show possible solutions of Equation (6) for systems with the range of parameters thought to be relevant to EXO 0748−676 (Parmar et al. 1986). In solving this equation we have ignored considerations of Roche lobe radii and stellar evolution and only constrained the accretion rate to the range found by Gottwald et al. (1986) in their analysis of X-ray bursts from the EXO 0748−676 system. The observed period derivative ($\dot{P}_{\rm orb} \sim 1.9 \times 10^{-11}$) requires a secondary mass less than that found by Parmar et al. (1986) in their analysis of the EXOSAT observations ($M_2 \sim 0.45 \, M_\odot$) but still within their allowed secondary mass range. However, this mass estimate was based on the assumption of the secondary star filling its Roche lobe and Equation (6) is derived without imposing this requirement. Thus, as long as we do not require any specific orbital geometry for the EXO 0748−676 system a positive $\dot{P}_{\rm orb}$ is allowed by simple theoretical considerations.

Negative values of $\dot{P}_{\rm orb}$ are the result of imposing on the LMXB models the additional constraints of Roche lobe geometry, stellar evolution of the binary components, and magnetic braking (e.g., Podsiadlowski et al. 2002 and references therein). Such models require that gravitational radiative angular momentum losses and magnetic braking conspire with the nuclear evolution of the secondary to slowly shrink the orbital separation and the secondary's Roche lobe resulting in mass transfer through the inner Lagrangian point. The negative $\dot{P}_{\rm orb}$ trend is maintained until the system attains an age near a Hubble time when a minimum

period is reached and $\dot{P}_{\rm orb}$ becomes positive as the orbital evolution is driven solely by gravitational radiation and the secondary is only a low mass degenerate helium star. A positive $\dot{P}_{\rm orb}$ before this final evolutionary epoch implies an expansion of the orbit radius and thus the Roche lobe radius, contrary to theoretical expectations. If one wishes to retain a gravitational radiation driven mass transfer model for the EXO 0748−676 system, the detailed models suggest you can not simultaneously reproduce the derived secondary mass and the observed orbit period while also meeting the observational requirement of a positive $\dot{P}_{\rm orb}$. Therefore, some additional physical mechanism other than the nuclear evolution of the secondary, angular momentum loss via gravitational radiation, or magnetic braking may be at work in the EXO 0748−676 system. However, if the secondary has a radius significantly less than its Roche lobe radius then some other mechanism besides Roche lobe overflow must be found to facilitate the observed mass transfer.

Howell et al. (2001) showed that as the secondary star in cataclysmic variables loses mass and evolves its outer envelope can be severely out of thermal equilibrium. This lack of equilibrium can result in the star becoming "bloated" in that it assumes a radius substantially larger than it would have if it were an isolated main sequence star of the same mass. This bloating can drive mass exchange between the system components even though a normal main sequence star of a mass equal to that of the secondary in EXO 0748−676 would have a radius substantially less than the Roche lobe radius and thus would not transfer substantial amounts of mass to the primary. Indeed, Howell et al. showed that this effect is greatest in the region of parameter space around $P_{\rm orb} \sim 3 - 4$ hours and $M_2 \sim 0.3 \ M_\odot$, very close to the expected EXO 0748−676 system parameters. Furthermore, if the system is rotating synchronously then the face of the secondary's surface oriented toward the primary is heated by X-rays generated by the accretion onto the compact object. This heating of the secondary's atmosphere may also lead to substantial mass transfer without the secondary being in contact with its Roche lobe (Ruderman et al. 1989; Harpaz & Rappaport 1991).

5.2. The Source of the Intrinsic Period Jitter

The time scale for both the circularization and synchronization of the EXO 0748−676 orbit is believed to be short compared to the binary evolutionary time scales (e.g. Zahn 1977). However, as Chandrasekhar (1963) has shown for a binary system consisting of two incompressible fluid masses in synchronous rotation, if the secondary's rotation rate is fast enough, significant distortions of the figure of the secondary can occur that are non-

axisymmetric. Chandrasekhar showed that as the value of

$$\alpha = \frac{\Omega^2}{\pi G \bar{\rho}}, \tag{7}$$

where $\bar{\rho}$ is the mean density of the secondary star and Ω is the angular frequency of the orbital motion, increases for a given mass ratio the equilibrium figure of the secondary becomes more extended along the line of centers under the influence of the tidal distortions induced by the primary. If we assume $M_1 = 1.4\,M_\odot$ and use $P_{\rm orb}$ to determine Ω then $\alpha \sim 0.13$ for any value of the secondary mass. Assuming $M_2 = 0.35\,M_\odot$ then from Table 1 of Chandrasekhar (1963) we find the secondary will be flattened by as much as 20% at the poles and the equatorial radius will be reduced in the direction perpendicular to the line of centers by as much as 10%. Thus, the figure of the secondary is distorted by strong departures from sphericity. Furthermore, Chandrasekhar shows that the effects of gas compressibility will be to enhance the instability in the secondary component's structure and this could lead to azimuthal instability modes being excited in the body of the secondary star. If azimuthal modes of oscillation are excited in the secondary star this can led to episodic periods of rapid mass transfer followed by periods of relatively quiescent mass transfer. Such oscillation modes need not rotate synchronously with the binary system, however, and this could result in the system occulting edge as observed from the earth significantly varying in distance from the system line of centers and thus causing us to observe seemingly non-systematic variations in the mid-eclipse times. Furthermore, the line of sight as we observe eclipses in EXO 0748−676 passes through the terminator on the secondary star's surface as seen from the X-ray production region. The terminator region is likely to be a region of significant disruption of the secondary's atmosphere, perhaps enough to also cause variations in the eclipse width as observed at the Earth.

Second, we have previously suggested (Paper II) that the star-spot cycle in the companion star can lead to changes in the quadrupole moment of the non-compact mass donating star. Angular momentum transfer will then cause variations in the orbital period apparently tied to some un-seen process occurring within the system. Transfer of angular momentum from the spin of the secondary to orbital motion will result in the secondary star being spun down. If the angular spin rate of the secondary is given by ω_2 then we can write the change in ω_2 corresponding to a change $P_{\rm orb}$ as

$$\Delta\omega_2 = \frac{1}{3} \frac{J_{\rm orb}}{I_2} \frac{\Delta P_{\rm orb}}{P_{\rm orb}} \tag{8}$$

where $I_2 = 2M_2 R_2^2/5$ is the moment of inertia of the secondary and R_2 is its radius. If the secondary is approximately tidally locked and we assume that R_2 is given by the Roche lobe radius for the secondary, using the stellar parameters given above this corresponds to

a change in spin frequency of $\Delta\omega_2 = 2.4 \times 10^{-9}$ Hz, or a fractional change of 5.6×10^{-6} in the spin frequency of the secondary.

However, if the secondary is significantly distorted from spherical by its tidal interaction with the primary then its moment of inertia will not be as simple as we assume above: I_2 will vary depending on which axis one considers. As mentioned above the X-rays from the mass accretion will asymmetrically heat the secondary's atmosphere. Convective currents in the secondary will try to redistribute some of the deposited heat energy around the star. These convective currents will redistribute angular momentum in the secondary away from the distribution that obtains for synchronous rotation. Enhanced tidal dissipation of energy associated with non-synchronous rotation will then be a continuous process for the secondary star. Also, due to the presence of the shadowing by the accretion disk around the compact object the secondary's atmospheric X-ray heating will vary strongly with latitude. As convection redistributes energy in the outer layers of the secondary this could give rise to differential rotation. Differential rotation of the secondary would increase the need for tidal dissipation of rotational energy in order to maintain synchronous system rotation. Furthermore, as large scale convective currents occur in the outer layers of the secondary star the moments of inertia for each axis of the secondary will vary by small amounts as mass is redistributed in a time-dependent fashion. Changes in one of the principle axes monents of inertia could result in the secondary star in EXO 0748−676 "wobbling" as it rotates in a manner similar to the "Chandler wobble" that occurs in the earth's polar motion as a result of azimuthal modes in the earth's interior (see Bursa & Pec 1993). Under these circumstances the O − C diagram for this system will never settle down into a smooth variation.

If the mass distribution in the donor is sufficiently disrupted so that its symmetry about the line of centers is affected then small changes in the apparent orbit period must be made in order to conserve angular momentum. If eclipses were purely geometric, then eclipse transitions are caused by the limb of the companion star. Changes in the atmosphere of the companion star which is the occulting edge for the sharp eclipse transitions, might account for the variable eclipse profiles (originally suggested by Parmar et al. 1991). Since the intrinsic jitter is only of the order ~ 0.1 s per eclipse any departures from a steady shape on the part of the secondary star need not be large. Assuming that $M_2 = 0.40\,M_\odot$ and the star's radius approaching its Roche lobe boundary, departures from spherical symmetry of order ~ 40 km will cause changes of ~ 0.1 s in the ingress or egress times. If the companion star changed shape or size in a manner which was symmetric about the line between the stars, then one would expect a correlation between the durations of ingress and egress. No such correlation is observed (Figure 9). If the companion star changed shape or size in a manner which was asymmetric about the same line and the figure of this shape change moves around the secondary with the same period as the rotation period of the star, then the observed

eclipse center would move away from the true eclipse center and the duration of the eclipse would change. However, no correlation is observed between mid-eclipse timing residuals and eclipse duration. On the other hand, if a non-axisymmetric distortion of the secondary's figure rotates with a period different from the secondary's rotation period then we might observe eclipse duration variations as we observe in EXO 0748−676. Such variations need not be in phase with the binary period if they result from instability modes that do not rotate around the center of the secondary in phase with the orbital period.

6. Conclusions

We have presented a three-fold increase in the total number of eclipse observations available for analysis of the orbital period from EXO 0748−676. These eclipse observations take advantage of the sub-second timing accuracy on the RXTE/PCA and ARGOS/USA experiments to determine mid-eclipse times to approximately 0.5 second accuracy. A linear ephemeris ($\dot{P}_{\rm orb} = 0$) and a quadratic ephemeris (non-zero $\dot{P}_{\rm orb}$) both give unacceptable fits to the eclipse center timing data. A maximum likelihood estimation model for the eclipse center timings that includes measurement error, intrinsic period jitter, and orbital period evolution is consistent with the data. We conclude that the true orbital period in EXO 0748−676 has increased by approximately 8 ms over the past 16 years. When we compare our results for $\dot{P}_{\rm orb}$ to those from theoretical models of LMXB evolution we find that the model $\dot{P}_{\rm orb}$'s have a different sign from our measured $\dot{P}_{\rm orb}$ for the EXO 0748−676 system.

The intrinsic period jitter, which has a magnitude of about 0.1 s per orbital cycle, causes the mid-eclipse times to do a random walk about the true solution. The atmosphere of the secondary star appears to not be a stable occulting edge on which to base eclipse center timings and thus its usage as an accurate fiducial marker of orbit evolution must now be questioned. Both the unexpected orbital evolution and the intrinsic period jitter may result from instabilities in the secondary star that are sufficient to slightly modify the system angular momentum distribution. Thus, the problem presented by the 8 ms change in the orbital period of EXO 0748−676 may be related to the problem of the origin of the intrinsic jitter in the mid-eclipse timings. We have suggested a number of possible enhancements to theoretical models of LMXB systems that may help solve both the problem of the unexpected positive orbit period derivative and the origin of the intrinsic jitter.

REFERENCES

Asai, K., Dotani, T., Nagase, F., Corbet, R. H. D., & Shaham, J. 1992, PASJ, 44, 633

Bursa, M. & Pec, K. 1993, Gravity Field and Dynamics of the Earth (New York: Springer-Verlag)

Chandrasekhar, S. 1963, ApJ, 138, 1182

Church, M. J., Balucinska-Church, M., Dotani, T., & Asai, K. 1998, ApJ, 504, 516

Cominsky, L. R. & Wood, K. S. 1984, ApJ, 283, 765

—. 1989, ApJ, 337, 485

Corbet, R. H. D., Asai, K., Dotani, T., & Nagase, F. 1994, ApJ, 436, L15

Deeter, J. E., Bonyton, P. E., Miyamoto, S., Kitamoto, S., Nagase, F., & Kawai, N. 1991, ApJ, 383, 324

Gottwald, M., Haberl, F., Parmar, A. N., & White, N. E. 1986, ApJ, 308, 213

—. 1987, ApJ, 323, 575

Harpaz, A. & Rappaport, S. 1991, ApJ, 383, 739

Heinz, S. & Nowak, M. A. 2001, MNRAS, 320, 249

Hertz, P., Ly, Y., Wood, K. S., & Cominsky, L. R. 1994, in The Evolution of X-Ray Binaries, (New York: AIP Press), 363

Hertz, P., Wood, K. S., & Cominsky, L. 1995, ApJ, 438, 385

Hertz, P., Wood, K. S., & Cominsky, L. R. 1997, ApJ, 486, 1000

Homan, J., Jonker, P. G., Wijnands, R., van der Klis, M., & van Paradijs, J. 1999, ApJ, 516, L91

Homan, J. & van der Klis, M. 2000, ApJ, 539, 847

Homer, L. & Charles, P. A. 1998, New Astronomy, 3, 435

Howell, S. B., Nelson, L. A., & Rappaport, S. 2001, ApJ, 550, 897

Jahoda, K., Swank, J. H., Giles, A. B., Stark, M. J., Strohmayer, T., Zhang, W., & Morgan, E. H. 1996, in Proc. SPIE, ed. O. H. Siegmund & M. A. Gummin, Vol. 2808, 59

Koen, C. 1996, MNRAS, 283, 471

Lombard, F. & Koen, C. 1993, MNRAS, 263, 309

Markwardt, C. B., Swank, J. H., & Strohmayer, T. E. 2002, in BAAS, Vol. 33, 1350

Oosterbroek, T., Parmar, A. N., Sidoli, L., in't Zand, J., & Heise, J. 2001, A&A, 376, 532

Parmar, A. N., Smale, A. P., Verbunt, F., & Corbet, R. H. D. 1991, ApJ, 366, 253

Parmar, A. N., White, N. E., Giommi, P., & Gottwald, M. 1986, ApJ, 308, 199

Podsiadlowski, P., Rappaport, S., & Pfahl, E. 2002, ApJ, 565, 1107

Press, W. H., Teukolsky, S. A., Vetterling, W. T., & Flannery, B. P. 1992, Numerical Recipes: The Art of Scientific Computing (New York: Cambridge University Press)

Rappaport, S., Joss, P. C., & Webbink, R. F. 1982, ApJ, 254, 616

Ray, P. S., Wood, K. S., Bandyopadhyay, R. M., Wolff, M. T., Fritz, G., Hertz, P., Kowalski, M. P., Lovellette, M. N., Yentis, D., Bloom, E. D., Godfrey, G., Focke, W., Giebels, B., Saz Parkinson, P., Reilly, K. T., Shabad, G., Titarchuk, L., Scargle, J., Backer, D., & Somer, A. 2000, BAAS, 32, 43.09

Ray, P. S., Wood, K. S., Fritz, G., Hertz, P., Kowalski, M., Johnson, W. N., Lovellette, M. N., Wolff, M. T., Yentis, D., Bandyopadhyay, R. M., Bloom, E. D., Giebels, B., Godfrey, G., Reilly, K., Saz Parkinson, P., Shabad, G., Michelson, P., Roberts, M., Leahy, D. A., Cominsky, L., Scargle, J., Beall, J., Chakrabarty, D., & Kim, Y. 2001, in AIP Conference Proceedings, Vol. 599, X-ray Astronomy 1999 – Stellar Endpoints, AGN, and the Diffuse Background, ed. G. Malaguti, G. Palumbo, & N. White (Melville, New York: AIP), 336

Rots, A. H., Jahoda, K., Macomb, D. J., Kawai, N., Saito, Y., Kaspi, V. M., Lyne, A. G., Manchester, R. N., Backer, D. C., Somer, A. L., Marsden, D., & Rothschild, R. E. 1998, ApJ, 501, 749

Ruderman, M., Shaham, J., Tavani, M., & Eichler, D. 1989, ApJ, 343, 292

Smale, A. P., Mukai, K., Williams, O. R., Jones, M. H., & Corbet, R. H. D. 1992, ApJ, 400, 330

Tavani, M. 1991, Nature, 351, 39

Thomas, B., Corbet, R., Smale, A. P., Asai, K., & Dotani, T. 1997, ApJ, 480, L21

van der Klis, M., Hasinger, G., Dotani, T., Mitsuda, K., Verbunt, F., Murphy, B. W., van Paradijs, J., Belloni, T., Makishima, K., Morgan, E., & Lewin, W. H. G. 1993, MNRAS, 260, 686

Verbunt, F. & van den Heuvel, E. P. J. 1995, in X-Ray Binaries, ed. W. H. G. Lewin, J. van Paradis, & E. P. J. van den Heuval, 457

Wachter, S. & Smale, A. P. 1998, ApJ, 496, L21

Wachter, S., Smale, A. P., & Bailyn, C. 2000, ApJ, 534, 367

White, N. E., Nagase, F., & Parmar, A. N. 1995, in X-Ray Binaries, ed. W. H. G. Lewin, J. van Paradis, & E. P. J. van den Heuval, 1

Wijnands, R., Strohmayer, T., & Franco, L. M. 2001, ApJ, 549, L71

Wood, K. S., Fritz, G., Hertz, P. L., Johnson, W. N., Lovellette, M. N., Ray, P. S., Wolff, M. T., Bandyopadhyay, R., Bloom, E. D., Chaput, C., Godfrey, G., Saz Parkinson, P., Shabad, G., Michelson, P., Roberts, M., Leahy, D. A., Cominsky, L., Scargle, J., Beall, J., Chakrabarty, D., & Kim, Y. 1999, BAAS, 31, 37.01

Zahn, J. P. 1977, A&A, 57, 383
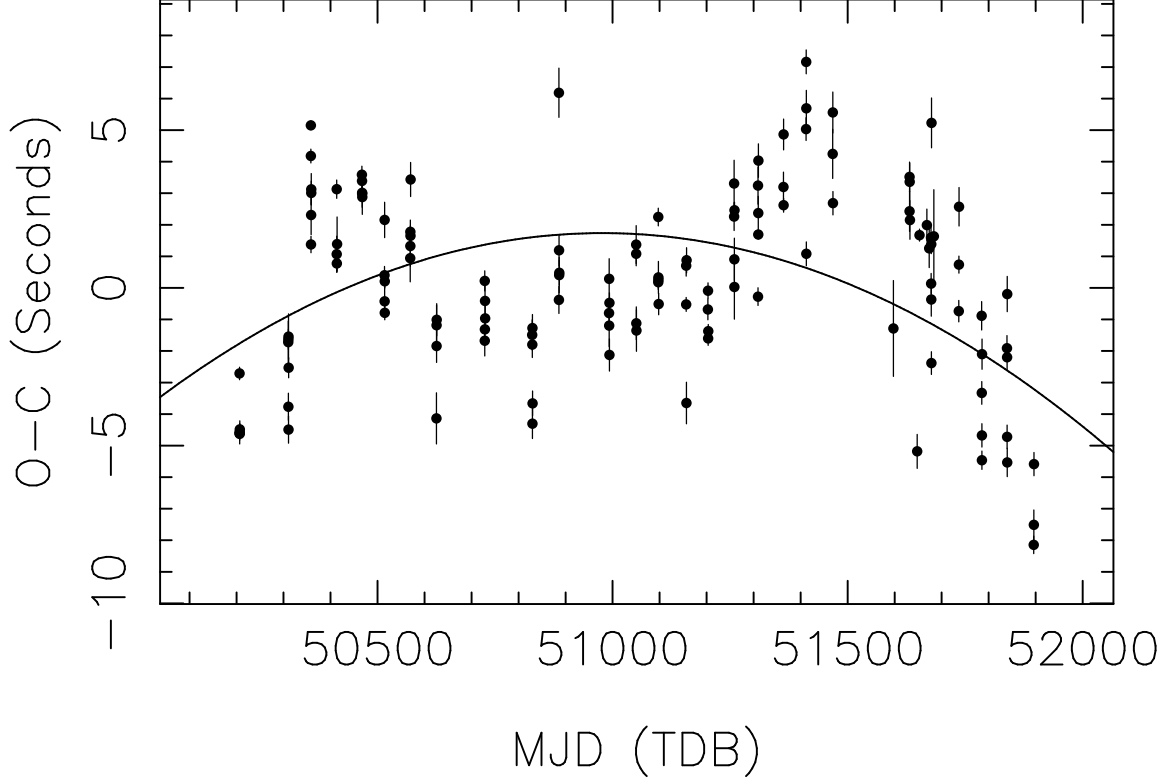
Fig. 1.— Mid-eclipse timing residuals for USA and RXTE observed eclipses of EXO 0748−676 during 1996−2000. The residual of the observed mid-eclipse time from a constant period of 0.15933781910 d and epoch of phase zero 46111.07418607 (MJD;TDB) is plotted as a function of barycenter corrected observation date. The curved line is the constant period derivative fit to the RXTE and USA data from Table 4. The residuals appear grouped both above and below the O − C = 0 baseline. The measurement errors are significantly less than the systematic wandering in the mid-eclipse times as was found in Paper II.
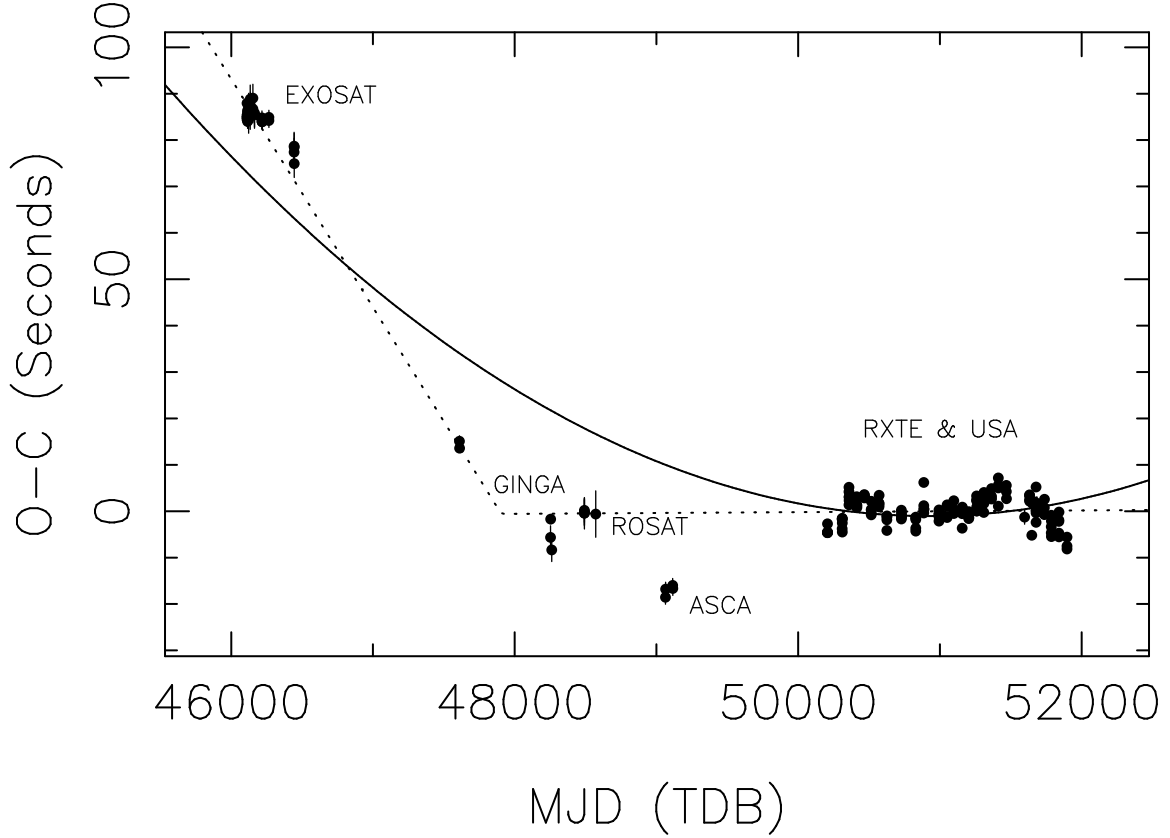
Fig. 2.— The mid-eclipse timing residuals for observed eclipses of EXO 0748−676 during 1985−2000 both from the present study and those available in the literature. The residual of the observed mid-eclipse time from the same constant period model as in Figure 1 is plotted as a function of barycenter corrected observation date. The curved solid line is the constant period derivative solution to all the data from Table 4. The dotted line is the broken constant period solution from Table 4. No simple linear or quadratic ephemeris fits all the data points.
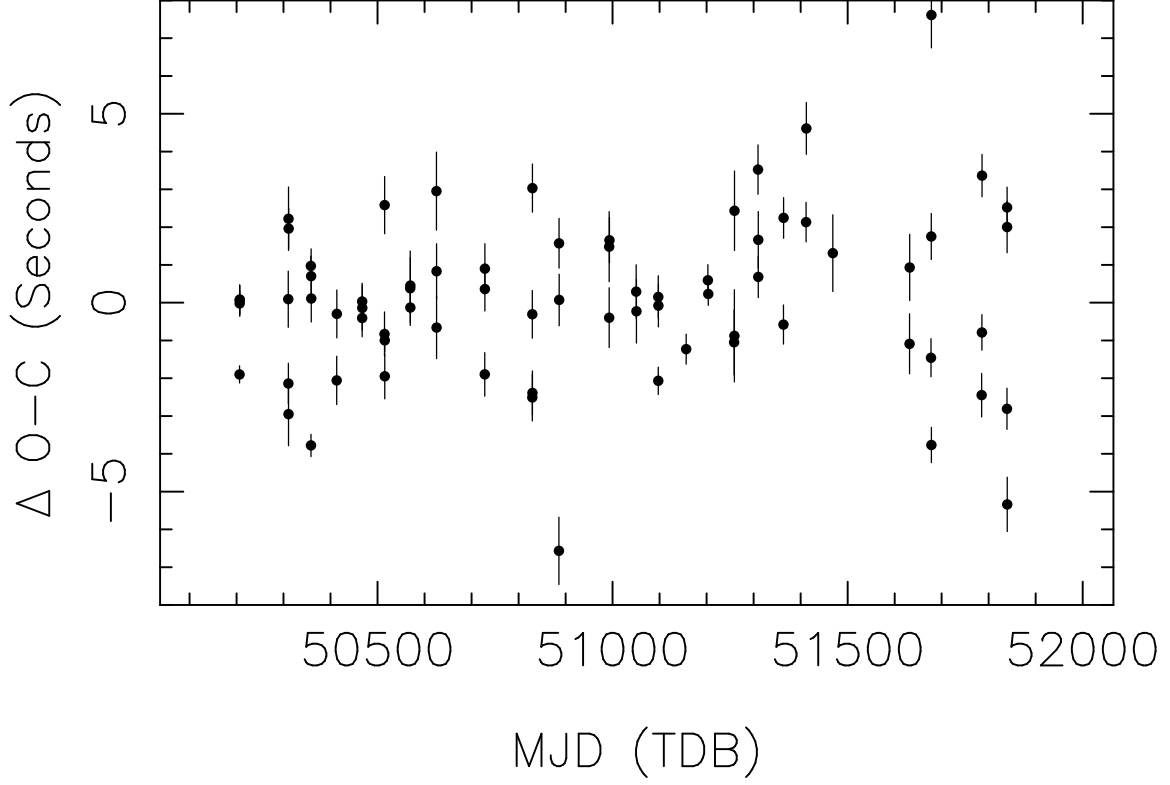
Fig. 3.— The difference in the O − C residuals for the case of consecutive observed eclipse cycles. We plot here $(O - C)_n - (O - C)_{n-1}$ when the observed eclipse cycle number n increases by 1.
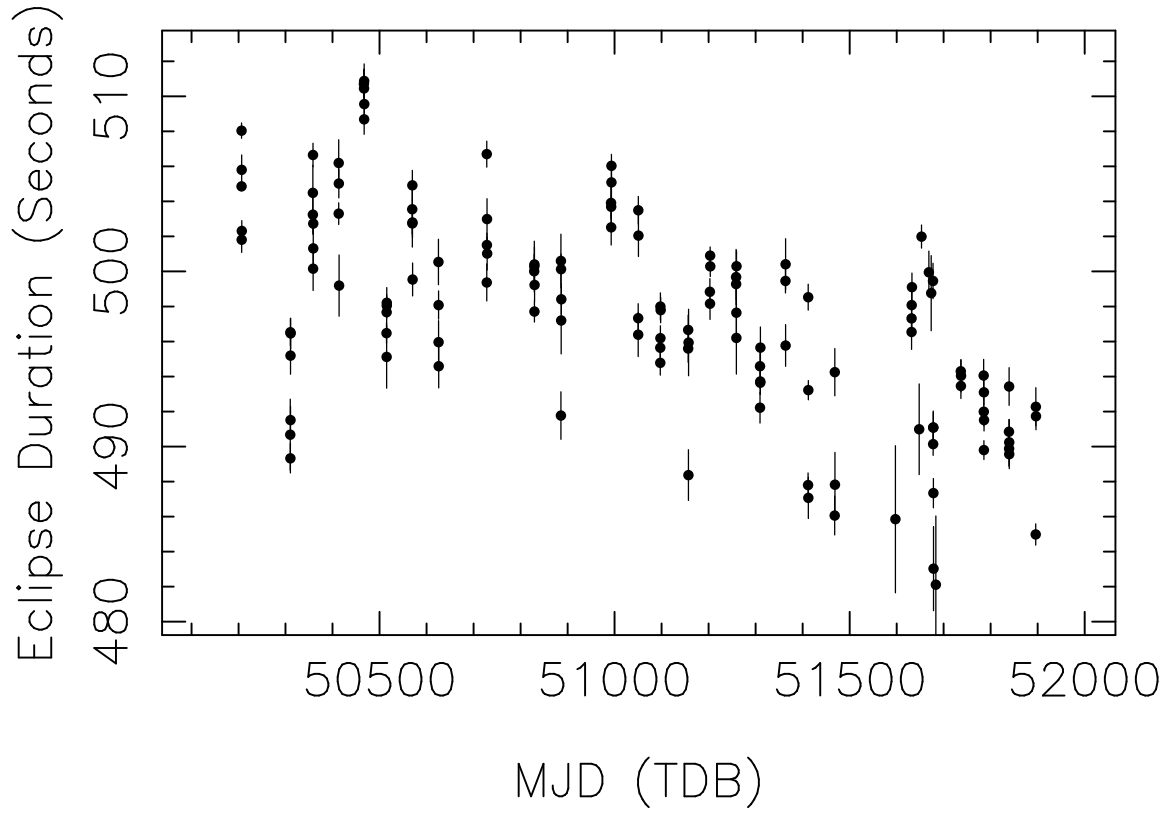
Fig. 4.— Eclipse duration of EXO 0748−676 during 1996−2000 as a function of observation date.
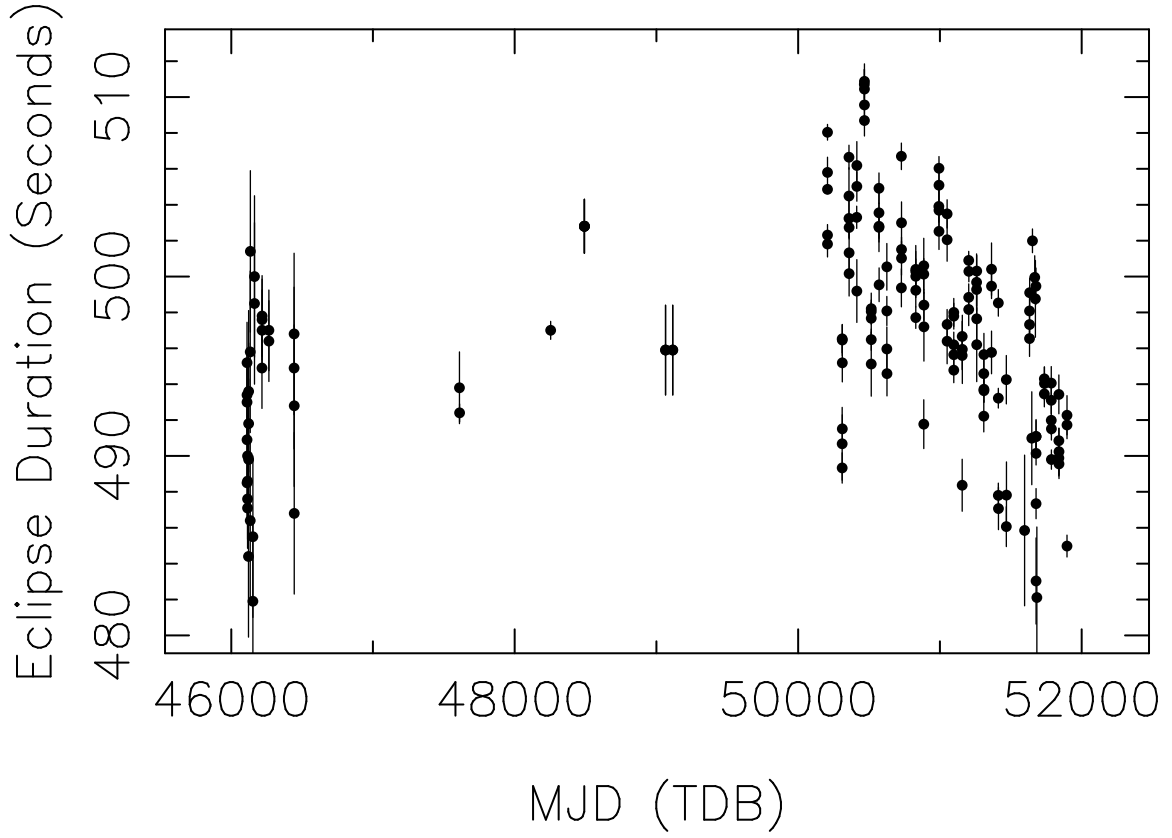
Fig. 5.— Eclipse duration of EXO 0748−676 during 1985−2000 as a function of observation date. Note that (i) the average eclipse duration was shorter in 1985−1986 than it was in 1996−1999, and (ii) the eclipse duration is variable during any epoch.
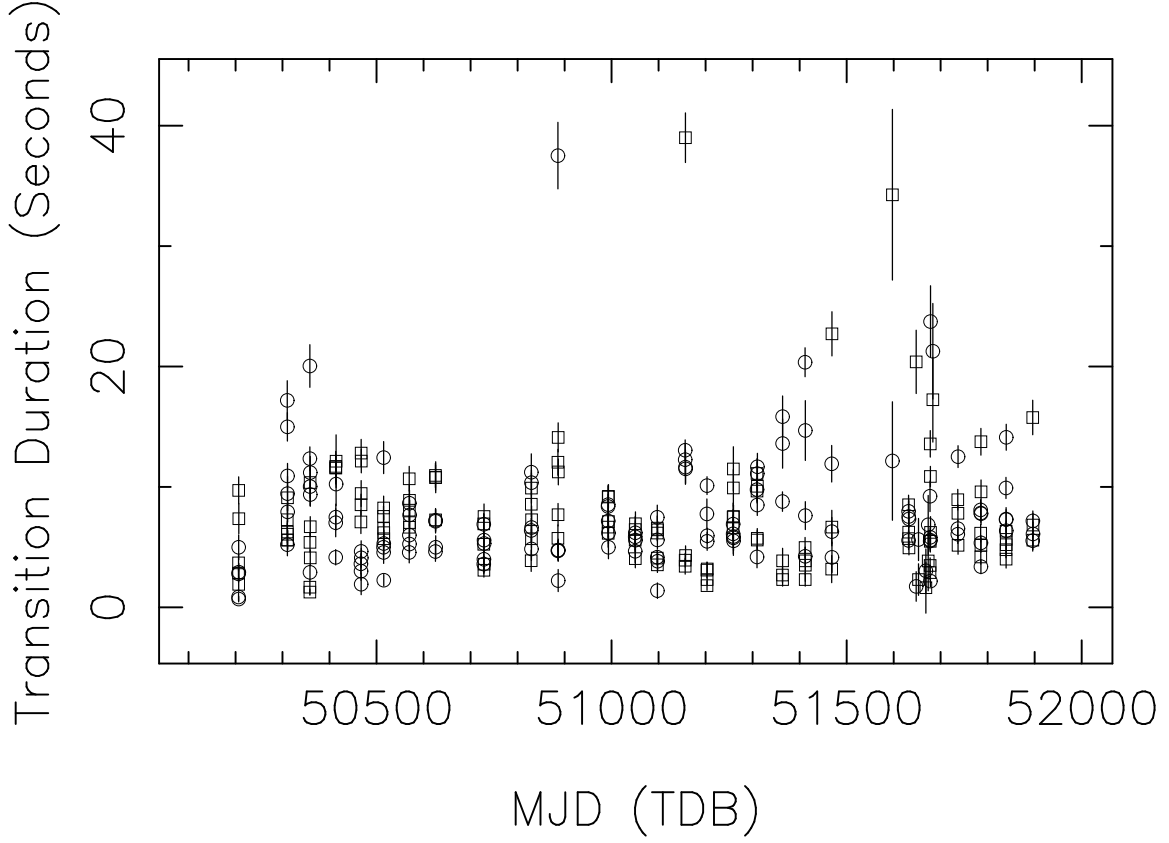
Fig. 6.— The duration of eclipse transitions (ingress and egress) for EXO 0748−676 as measured by USA and RXTE as a function of observation date for observations during 1996−2000. The circles show the durations of ingress and the squares show the durations of egress. The duration of ingress and egress are significantly variable, even for consecutive eclipses.
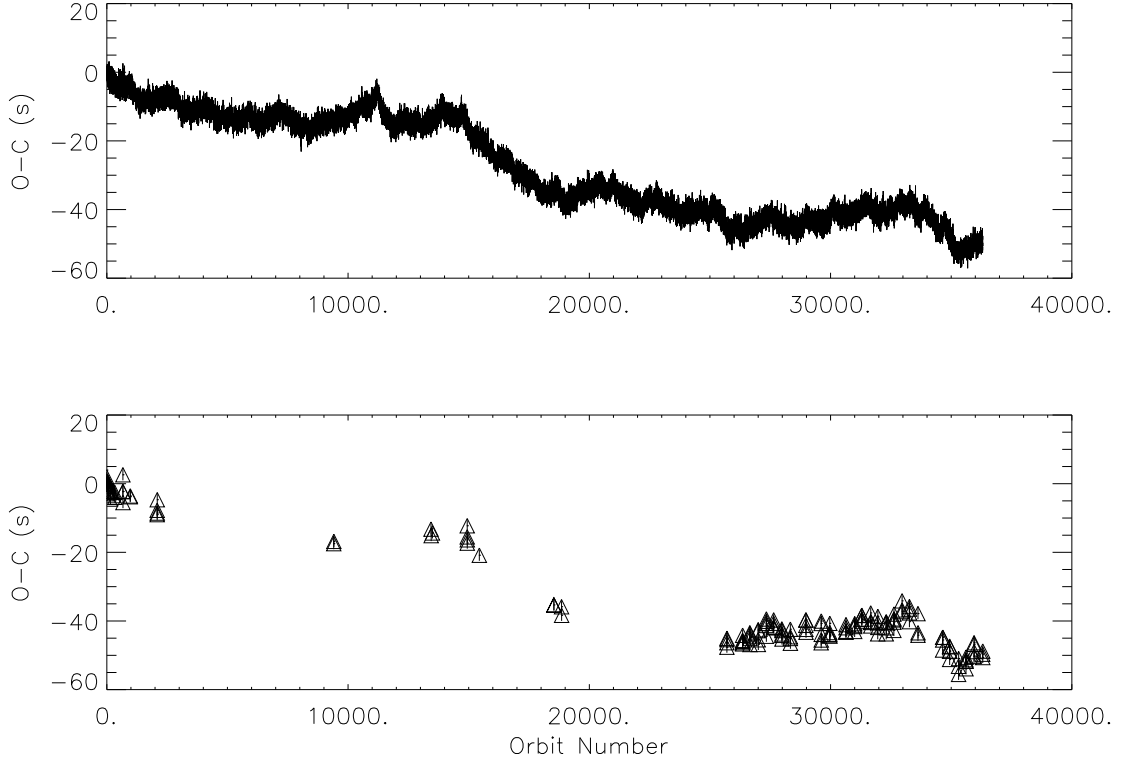
Fig. 7.— Example output from Monte Carlo simulation of a random process following Equation 1 with no true orbital period derivative. The parameters used are those derived from the actual data ($\sigma_\epsilon = 0.105$ s and $\sigma_e = 1.62$ s). The top frame shows the simulated mid-eclipse times for every eclipse, while the bottom frame shows the same data but sampled using the sampling function of the actual observational data. Notice how simple fitting of short spans of data can easily detect spurious positive or negative period derivatives even though none actually exists in this case.
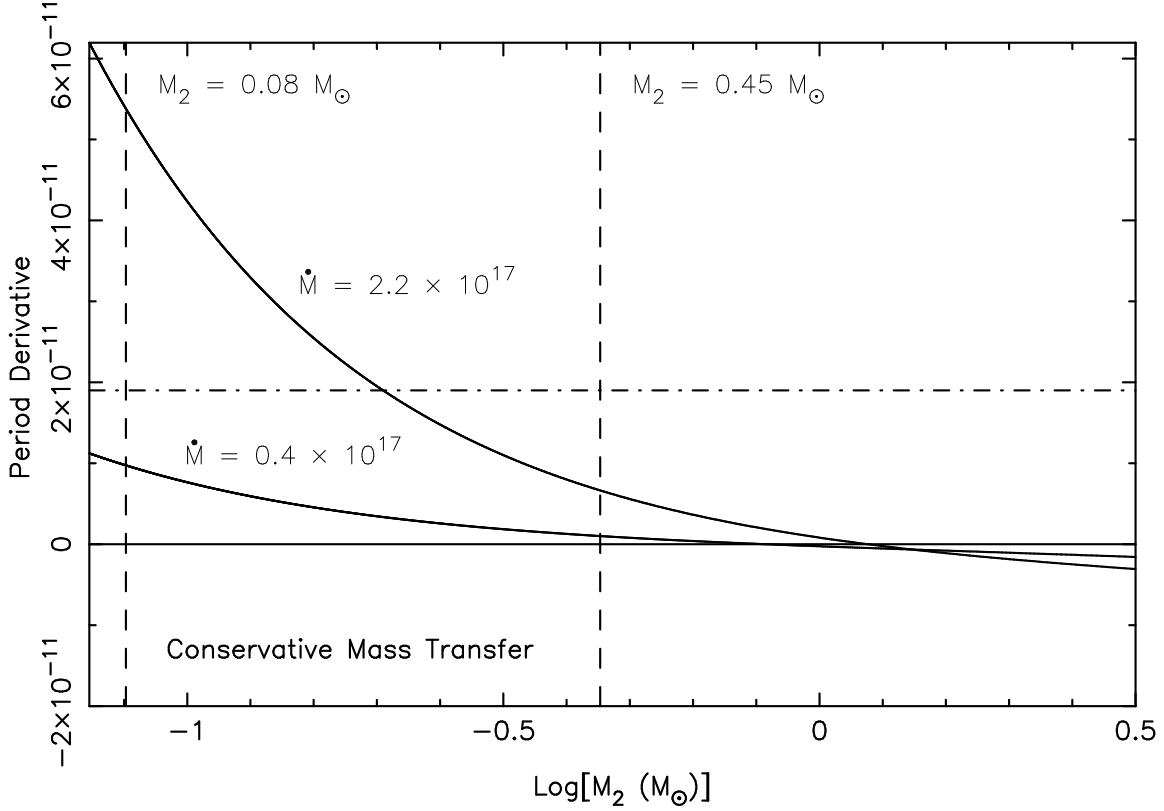
Fig. 8.— The possible values of the period derivative $\dot{P}_{\mathrm{orb}}$ as a function of the secondary mass M_2. The curved solid lines represent the limits placed on the accretion rate by Gottwald et al. (1986, $\dot{M}_1 = 0.4 - 2.2 \times 10^{17} \mathrm{g\ s^{-1}}$) in their analysis of X-ray bursts from EXO 0748−676. We assume a 1.4 $M_\odot$ neutron star with radius 10 km. The vertical dashed lines show the best fit secondary mass range derived by Parmar et al. (1986): $M_2 = 0.08 - 0.45\,M_\odot$. The horizontal dot-dashed line represents $\dot{P}_{\mathrm{orb}} = 1.9 \times 10^{-11}$.
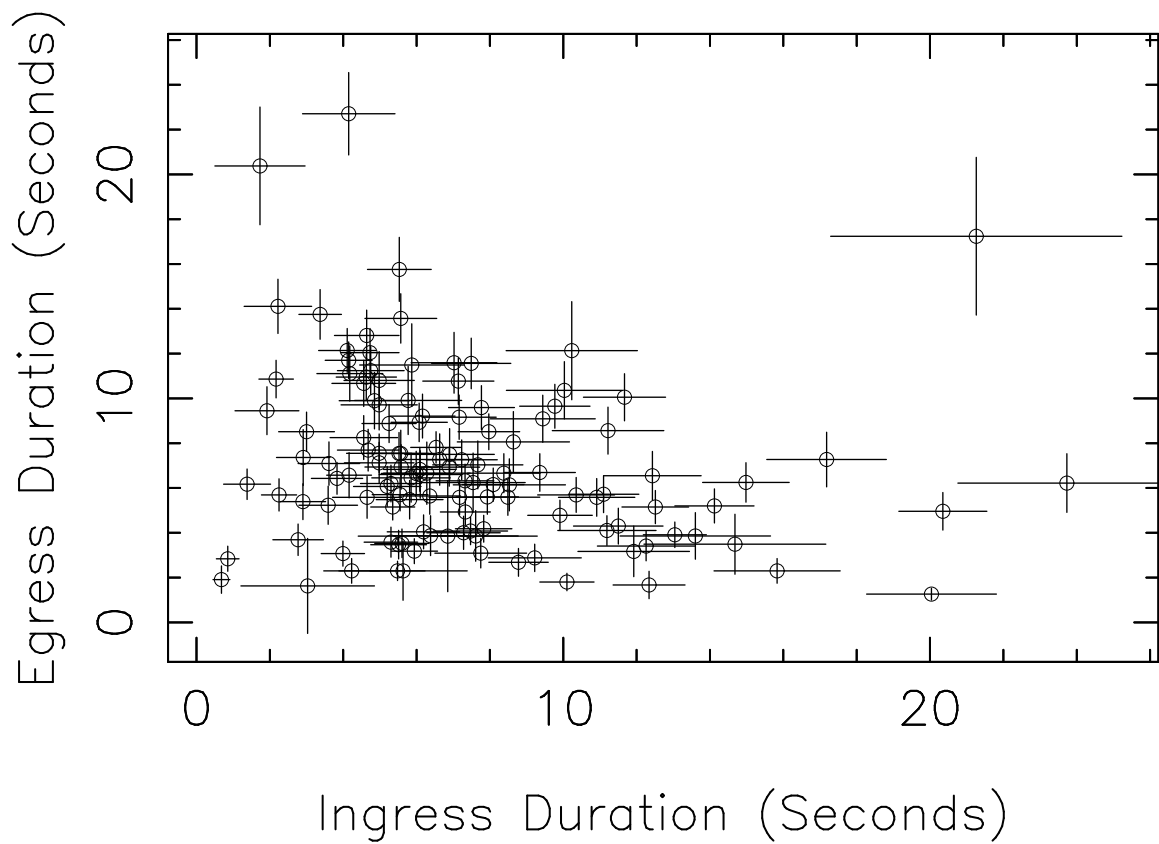
Fig. 9.— The duration of eclipse egress plotted against the duration of eclipse ingress for EXO 0748−676 as measured by USA and RXTE for observations made during 1996−2000.

Table 1. **RXTE Timing of Full EXO 0748−676 Eclipses**

RXTE ObsID	Cycle Number	Mid-Eclipse Time (JD;TDB)	Timing Uncertainty (s)
10108-01-01	25702	2450206.87478130	0.20
10108-01-02	25703	2450207.03409715	0.11
10108-01-03	25704	2450207.19343477	0.32
10108-01-04	25705	2450207.35277331	0.26
10108-01-05	25706	2450207.51211208	0.27
10108-01-06	26353	2450310.60371301	0.67
10108-01-07	26354	2450310.76305190	0.32
10108-01-08	26355	2450310.92236498	0.43
10108-01-09	26356	2450311.08172852	0.72
10108-01-10	26357	2450311.24103222	0.43
10108-01-07-01	26358	2450311.40039275	0.32
10108-01-11	26654	2450358.56446486	0.22
10108-01-12	26655	2450358.72381394	0.14[a]
10108-01-13	26656	2450358.88310803	0.26
10108-01-14	26658	2450359.20179449	0.62
10108-01-15	26659	2450359.36114044	0.37
10108-01-15-01	26660	2450359.52047956	0.50
20069-01-01	26999	2450413.53600028	0.29
20069-01-02	27000	2450413.69531428	0.57
20069-01-03	27001	2450413.85464866	0.28
20069-01-05	27004	2450414.33266926	0.86
20069-02-01	27336	2450467.23285063	0.27
20069-02-02	27338	2450467.55152400	0.24
20069-02-03	27339	2450467.71085711	0.43
20069-02-04	27340	2450467.87019530	0.22
20069-02-05	27341	2450468.02953153	0.55
20069-03-01	27638	2450515.35283512	0.28
20069-03-02	27639	2450515.51216336	0.51
20069-03-03	27640	2450515.67153106	0.56
20069-03-04	27641	2450515.83084634	0.21

Table 1—Continued

RXTE ObsID	Cycle Number	Mid-Eclipse Time (JD;TDB)	Timing Uncertainty (s)
20069-03-05	27642	2450515.99017262	0.22
20069-04-01	27981	2450570.00571336	0.75
20069-04-02	27982	2450570.16505560	0.64
20069-04-03	27983	2450570.32439866	0.37
20069-04-04	27984	2450570.48373500	0.15
20069-04-05	27986	2450570.80243130	0.54
20069-05-01	28331	2450625.77389125	0.81
20069-05-02	28332	2450625.93326324	0.64
20069-05-03	28333	2450626.09259345	0.52
20069-05-04	28334	2450626.25194090	0.51
20069-06-01	28976	2450728.54683500	0.32
20069-06-02	28977	2450728.70615086	0.48
20069-06-03	28978	2450728.86549287	0.33
20069-06-04	28979	2450729.02484113	0.57
20069-06-05	28981	2450729.34351035	0.43
30067-01-01	29610	2450829.56699252	0.48
30067-01-02	29611	2450829.72632678	0.41
30067-01-03	29612	2450829.88563558	0.47
30067-01-04	29613	2450830.04500850	0.43
30067-01-05	29614	2450830.20431868	0.39
30067-02-01	29966	2450886.29134495	0.78[a]
30067-02-02	29967	2450886.45060676	0.43
30067-02-03	29968	2450886.60996278	0.50
30067-02-04	29970	2450886.92862933	0.56
30067-02-05	29971	2450887.08796799	0.39
30067-03-01	30636	2450993.04760294	0.42
30067-03-02	30637	2450993.20693616	0.67
30067-03-03	30638	2450993.36629113	0.64
30067-03-04	30640	2450993.68493882	0.51
30067-03-05	30641	2450993.84429576	0.32

Table 1—Continued

RXTE ObsID	Cycle Number	Mid-Eclipse Time (JD;TDB)	Timing Uncertainty (s)
30067-04-01	30997	2451050.56857736	0.38
30067-04-02	30998	2451050.72791856	0.60
30067-04-04	31000	2451051.04656532	0.52
30067-04-05	31001	2451051.20590051	0.66
30067-05-01	31292	2451097.57324750	0.28
30067-05-02	31293	2451097.73256139	0.23
30067-05-03	31294	2451097.89190097	0.51
30067-05-04	31295	2451098.05123789	0.24
30067-05-05	31297	2451098.36990468	0.34
30067-06-01	31665	2451157.00623616	0.33
30067-06-02	31666	2451157.16555977	0.22
30067-06-03	31668	2451157.48419924	0.66
30067-06-05	31670	2451157.80292725	0.40
40039-01-01	31955	2451203.21418766	0.33[a]
40039-01-02	31956	2451203.37353234	0.25
40039-01-04	31959	2451203.85152829	0.22
40039-01-05	31960	2451204.01086880	0.21
40039-02-01	32305	2451258.98247053	0.74
40039-02-02	32306	2451259.14179623	0.44
40039-02-03	32308	2451259.46045618	0.67
40039-02-04	32309	2451259.61978384	1.02
40039-02-05	32310	2451259.77914981	0.26
40039-03-01	32624	2451309.81119333	0.28
40039-03-02	32625	2451309.97057192	0.59
40039-03-03	32627	2451310.28922956	0.14
40039-03-04	32628	2451310.44857528	0.53
40039-03-05	32629	2451310.60793234	0.53
40039-04-01	32964	2451363.98609206	0.47
40039-04-02	32965	2451364.14542319	0.22
40039-04-03	32966	2451364.30478697	0.49

Table 1—Continued

RXTE ObsID	Cycle Number	Mid-Eclipse Time (JD;TDB)	Timing Uncertainty (s)
40039-05-02	33266	2451412.10613465	0.36
40039-05-03	33267	2451412.26549715	0.38
40039-05-04	33269	2451412.58410236	0.38
40039-05-05	33270	2451412.74349356	0.57
40039-06-02	33622	2451468.83038917	0.78
40039-06-03	33623	2451468.98974218	0.65
40039-06-04	33625	2451469.30838454	0.37
50045-01-01	34647	2451632.15164530	0.47
50045-01-02	34648	2451632.31097053	0.64
50045-01-03	34649	2451632.47031914	0.60
50045-01-05	34652	2451632.94831856	0.61
50045-02-01	34934	2451677.88157713	0.39
50045-02-02	34935	2451678.04089808	0.32
50045-02-03	34937	2451678.35956787	0.53
50045-02-04	34938	2451678.51892597	0.30
50045-02-05	34939	2451678.67822018	0.36
50045-03-01	35304	2451736.83654322	0.34
50045-03-03	35306	2451737.15523593	0.27
50045-03-04	35308	2451737.47393280	0.61
50045-04-01	35610	2451785.59391417	0.45
50045-04-02	35611	2451785.75322366	0.36
50045-04-04	35613	2451786.07188373	0.37
50045-04-05	35614	2451786.23121243	0.29
50045-04-06	35615	2451786.39058917	0.48
50045-05-01	35948	2451839.45008512	0.40
50045-05-02	35949	2451839.60939044	0.37
50045-05-03	35950	2451839.76875745	0.39
50045-05-04	35951	2451839.92811845	0.56
50045-05-05	35952	2451840.08739449	0.45
50045-06-01	36305	2451896.33361440	0.28

Table 1—Continued

RXTE ObsID	Cycle Number	Mid-Eclipse Time (JD;TDB)	Timing Uncertainty (s)
50045-06-03	36307	2451896.65229738	0.47
50045-06-04	36309	2451896.97099530	0.37

[a]Analysis time binning is 1.0 seconds for this ObsID.

Table 2. **USA Timing of Full EXO 0748−676 Eclipses**

USA ObsID	Cycle Number	Mid-Eclipse Time (JD;TDB)	Timing Uncertainty (s)
D054-091610-093531	34432	2451597.89395861	1.52
D105-011351-014146	34750	2451648.56333998	0.54
D109-234506-001510	34781	2451653.50289171	0.19
D125-104356-094101	34878	2451668.95866382	0.51
D130-091628-081414	34909	2451673.89812771	0.61
D135-074949-064725	34940	2451678.83764611	0.79[a]
D140-062245-064725	34971	2451683.77707690	1.48

[a]Analysis time binning is 2.0 seconds for this ObsID.

Table 3. **Other Satellite Timing Data of Full EXO 0748−676 Eclipses**

Satellite	Reference	Cycle Number	Mid-Eclipse Time (JD;TDB)	Timing Uncertainty (s)
EXOSAT	Parmar et al. 1991	1	2446111.734512	1.5
EXOSAT	Parmar et al. 1991	2	2446111.893839	1.5
EXOSAT	Parmar et al. 1991	3	2446112.053182	1.5
EXOSAT	Parmar et al. 1991	4	2446112.212520	1.5
EXOSAT	Parmar et al. 1991	5	2446112.371893	1.5
EXOSAT	Parmar et al. 1991	25	2446115.558604	1.5
EXOSAT	Parmar et al. 1991	26	2446115.717969	1.5
EXOSAT	Parmar et al. 1991	27	2446115.877285	1.5
EXOSAT	Parmar et al. 1991	28	2446116.036640	1.5
EXOSAT	Parmar et al. 1991	70	2446122.728826	3.0
EXOSAT	Parmar et al. 1991	71	2446122.888149	3.0
EXOSAT	Parmar et al. 1991	72	2446123.047517	3.0
EXOSAT	Parmar et al. 1991	73	2446123.206835	3.0
EXOSAT	Parmar et al. 1991	146	2446134.838536	3.0
EXOSAT	Parmar et al. 1991	147	2446134.997833	3.0
EXOSAT	Parmar et al. 1991	148	2446135.157194	3.0
EXOSAT	Parmar et al. 1991	263	2446153.481063	3.0
EXOSAT	Parmar et al. 1991	264	2446153.640374	3.0
EXOSAT	Parmar et al. 1991	332	2446164.475332	3.0
EXOSAT	Parmar et al. 1991	333	2446164.634673	3.0
EXOSAT	Parmar et al. 1991	666	2446217.694155	1.5
EXOSAT	Parmar et al. 1991	667	2446217.853483	1.5
EXOSAT	Parmar et al. 1991	668	2446218.012821	1.5
EXOSAT	Parmar et al. 1991	669	2446218.172160	1.5
EXOSAT	Parmar et al. 1991	971	2446266.292183	1.5
EXOSAT	Parmar et al. 1991	972	2446266.451529	1.5
EXOSAT	Parmar et al. 1991	2088	2446444.272463	3.0
EXOSAT	Parmar et al. 1991	2089	2446444.431786	3.0
EXOSAT	Parmar et al. 1991	2090	2446444.591136	3.0
EXOSAT	Parmar et al. 1991	2091	2446444.750433	3.0

Table 3—Continued

Satellite	Reference	Cycle Number	Mid-Eclipse Time (JD;TDB)	Timing Uncertainty (s)
GINGA	Asai et al. 1992	9406	2447610.305887	1.2
GINGA	Parmar et al. 1991	9411	2447611.102559	0.4
GINGA	Asai et al. 1992	13438	2448252.755734	2.5
GINGA	Asai et al. 1992	13446	2448254.030482	1.0
GINGA	Asai et al. 1992	13496	2448261.997296	2.5
GINGA	Asai et al. 1992	14939	2448491.921868	2.6
GINGA	Asai et al. 1992	14940	2448492.081202	2.8
GINGA	Asai et al. 1992	14941	2448492.240537	2.8
GINGA	Asai et al. 1992	14942	2448492.399874	3.4
ROSAT	Hertz et al. 1994	15440	2448571.750106	5.0
ASCA	Corbet et al. 1994	18532	2449064.422435	1.5
ASCA	Corbet et al. 1994	18533	2449064.581793	1.5
ASCA	Corbet et al. 1994	18850	2449115.091891	1.5
ASCA	Corbet et al. 1994	18852	2449115.410559	1.5

Table 4. **Orbital Ephemerides of EXO 0748−676**

Parameter		Value
Constant Period Ephemeris: $T_n = T_0 + nP_{\rm orb}$ RXTE and USA Data Only		
T_0 (MJD/TDB)	$=$	$46111.07418607 \pm 0.0000030$
$P_{\rm orb}$ (day)	$=$	$0.15933781910 \pm 0.00000000010$
χ^2(dof)	$=$	$84.8(127)$
Quadratic Ephemeris: $T_n = T_0 + nP_{\rm orb} + \frac{1}{2}n^2 P_{\rm orb}\dot{P}_{\rm orb}$ RXTE and USA Data Only		
T_0 (MJD/TDB)	$=$	$46111.072596 \pm 0.000034$
$P_{\rm orb}$ (day)	$=$	$0.1593379245 \pm 0.0000000022$
$\dot{P}_{\rm orb}$	$=$	$(-2.17 \pm 0.05) \times 10^{-11}$
τ_{orb} (yr)	$=$	2.0×10^7
χ^2(dof)	$=$	$68.0(126)$
Quadratic Ephemeris: $T_n = T_0 + nP_{\rm orb} + \frac{1}{2}n^2 P_{\rm orb}\dot{P}_{\rm orb}$ All Data		
T_0 (MJD/TDB)	$=$	$46111.0750313 \pm 0.0000037$
$P_{\rm orb}$ (day)	$=$	$0.15933776231 \pm 0.00000000027$
$\dot{P}_{\rm orb}$	$=$	$(1.181 \pm 0.007) \times 10^{-11}$
τ_{orb} (yr)	$=$	3.7×10^7
χ^2(dof)	$=$	$121.1(170)$
Broken Constant Period Ephemeris: $T_n = \begin{cases} T_0 + nP_{\rm orb,0} & \text{if } n < n_{break} \\ T_0 + n_{break}P_{\rm orb,0} + (n - n_{break})P_{\rm orb,1} & \text{if } n \geq n_{break} \end{cases}$ All Data		
T_0 (MJD/TDB)	$=$	$46111.0752008 \pm 0.0000042$
$P_{\rm orb,0}$ (day)	$=$	$0.15933772839 \pm 0.00000000066$
n_{break} (cycle)	$=$	11260.8 ± 62.2
$P_{\rm orb,1}$ (day)	$=$	$0.159337819444 \pm 0.000000000098$
χ^2(dof)	$=$	$67.3(169)$

Table 5.   **Maximum Likelihood Estimators for EXO 0748−676 Orbital Ephemeris**

Parameter	Full Model	NO Period Change	NO Intrinsic Noise
All Data			
Log Likelihood	1576.8254	1571.7447	1372.9745
P_{orb}(day)	0.1593377355	0.1593377897	0.1593377395
Δ (day)	2.99×10^{-12}	...	3.02×10^{-12}
q	0.009087	0.01312	...
σ_e^2 (s^2)	2.34	2.29	49.4
$\dot{P}_{\mathrm{orb}}$	1.87×10^{-11}	...	1.89×10^{-11}
τ_{orb} (yr)	2.3×10^7	...	2.3×10^7
σ_e (s)	1.53	1.51	7.03
σ_ϵ (s)	0.146	0.173	...
RXTE and USA Data Only			
Log Likelihood	1179.7571	1178.3791	1141.2872
P_{orb}(day)	0.1593380321	0.1593378164	0.1593379030
Δ (day)	-6.96×10^{-12}	...	-2.71×10^{-12}
q	0.004341	0.005316	...
σ_e^2 (s^2)	2.66	2.62	7.58
$\dot{P}_{\mathrm{orb}}$	-4.37×10^{-11}	...	-1.70×10^{-11}
τ_{orb} (yr)	1.0×10^7	...	2.6×10^7
σ_e (s)	1.63	1.62	2.75
σ_ϵ (s)	0.107	0.118	...